



HAL
open science

Analysis of multisite 2D relaxation exchange NMR

Maxime van Landeghem, Agnes Haber, Jean-Baptiste d'Espinose de
Lacaillerie, Bernhard Blümich

► **To cite this version:**

Maxime van Landeghem, Agnes Haber, Jean-Baptiste d'Espinose de Lacaillerie, Bernhard Blümich. Analysis of multisite 2D relaxation exchange NMR. Concepts in Magnetic Resonance Part A: Bridging Education and Research, 2010, 36A (3), pp.153-169. 10.1002/cmr.a.20157 . hal-03984429

HAL Id: hal-03984429

<https://hal.science/hal-03984429>

Submitted on 12 Feb 2023

HAL is a multi-disciplinary open access archive for the deposit and dissemination of scientific research documents, whether they are published or not. The documents may come from teaching and research institutions in France or abroad, or from public or private research centers.

L'archive ouverte pluridisciplinaire **HAL**, est destinée au dépôt et à la diffusion de documents scientifiques de niveau recherche, publiés ou non, émanant des établissements d'enseignement et de recherche français ou étrangers, des laboratoires publics ou privés.

Analysis of Multisite 2D Relaxation Exchange NMR

MAXIME VAN LANDEGHEM,^{1,2,3} AGNES HABER,¹
JEAN-BAPTISTE D'ESPINOSE DE LACAILLERIE,² BERNHARD BLÜMICH¹

¹*Institute of Technical and Macromolecular Chemistry, RWTH Aachen University, D-52056 Aachen, Germany*

²*Science et Ingénierie de la Matière Molle, UMR 7615 CNRS UPMC, ESPCI ParisTech, 10 rue Vauquelin, 75005 Paris, France*

³*Saint-Gobain Recherche, 39 quai Lucien Lefranc, BP 135, 93303 Aubervilliers, France*

ABSTRACT: Two-dimensional (2D) relaxation exchange nuclear magnetic resonance (NMR) is in many ways similar to 2D frequency exchange NMR, except that the encoding times are comparable to the exchange time. This fact prevents the straightforward analysis of the cross-peak intensities in terms of joint probability densities, and quantitative information and understanding can only be obtained by comparison with simulated spectra. Based on simulations, an explanation is proposed as to why interference between relaxation and exchange may lead to asymmetric 2D exchange maps when exchange occurs between more than two sites. Practically, retro-fitting a simulated data set to an experimental one is shown to allow for the determination of the experimental relaxation and exchange parameters. This point is illustrated by studying a two-site model system consisting of interstitial water exchanging within a pack of spherical silica particles. © 2010 Wiley Periodicals, Inc. Concepts Magn Reson Part A 36A: 153–169, 2010.

KEY WORDS: NMR; Laplace inversion; exchange NMR; porous materials

I. INTRODUCTION

Two-dimensional (2D) relaxation exchange NMR is a form of 2D nuclear magnetic resonance (NMR) where molecular motion and transport are mapped by relaxation exchange. This NMR technique is now gaining momentum in a wide variety of applications involving wetting and drying of liquids in porous

media (1–7). This experiment is analogous to 2D frequency exchange NMR but appears more appropriate for the study of the exchange of liquids between pores because relaxivity is expected to depend on pore size, whereas the chemical shift is not (8).

2D Fourier transform frequency exchange NMR spectroscopy (9) is one of the many forms of correlation NMR (10–12), which reveals dynamic processes on the time scale of the longitudinal relaxation time T_1 . The principle is simple and elegant. During a first period t_1 , a chemical group is in a particular chemical environment resulting in a given NMR frequency ω_1 . This frequency is encoded by recording the corresponding free induction decay (FID) of the magnetization. Then, it exchanges for another chemical environment of NMR frequency ω_2 during a time lag t_m , while the magnetization evolution is frozen by

Received 26 November 2009; revised 8 April 2010; accepted 11 April 2010

Correspondence to: Jean-Baptiste d'Espinose de Lacaillierie;
E-mail: jean-baptiste.despinose@espci.fr

Concepts in Magnetic Resonance Part A, Vol. 36A(3) 153–169 (2010)

Published online in Wiley InterScience (www.interscience.wiley.com). DOI 10.1002/cmra.20157

© 2010 Wiley Periodicals, Inc.

aligning the magnetization with the direction of the polarizing field. Finally, the FID is measured during a period starting at time $t = t_1 + t_m$. Ideally, magnetization is transferred during the mixing time t_m from one site (with a given magnetic environment identified by an initial frequency ω_1 measured during the evolution period t_1) to another site (with a different magnetic environment identified by a final frequency ω_2 , which is measured during the detection period t_2). Such a transfer can arise, for example, from translational and rotational motion of molecules, rotations or jumps of chemical groups about bonds, and from cross relaxation (11). After 2D Fourier transformation, a correlation map is obtained, which unravels the transfer pathways. From a series of such maps acquired with different mixing times, the exchange rates can be deduced (13).

This type of analysis is popular in NMR spectroscopy, because many different sites can be discriminated in terms of their chemical shifts in an NMR spectrum (14). It remains experimentally demanding, however, because to measure a chemical shift spectrum, a highly homogeneous magnetic field is needed, which requires a sophisticated magnet. Yet, the nuclear magnetic response of a molecule to a particular environment is not only characterized by a chemical shift but also by a rate of decay. Conceptually, the chemical shift scale can be replaced by a relaxation or a diffusion scale, so that the occupancy of the different sites is obtained not by the structure of the frequency distribution but instead by the distribution of relaxation rates or diffusion coefficients. In practice, only three or four different sites can usually be resolved on a relaxation or diffusion scale, but this disadvantage is largely compensated by the fact that magnetization decay measurements can easily be obtained with simple magnets and inhomogeneous fields. This concept of relaxation exchange NMR is not new (15, 16), but it has gained recent popularity with the development of a stable 2D inverse Laplace transformation (ILT) algorithm (17), a development reminiscent of Fourier NMR that gained momentum only once the fast Fourier Transformation algorithm had been mastered by the NMR community (5, 18).

Despite the fact that relaxation measurements can be executed with simple hardware and that they do not require a homogeneous magnet, 2D Laplace NMR (1, 19–21) did not develop as early as the spectroscopic study of motion by 2D Fourier exchange NMR. There are two likely reasons for this delay. First, the inversion of the data from the time domain into the relaxation rate domain involves the ill-defined ILT (17, 22), which generates artifacts that are not as well understood as the ones coming from

the Fourier transformation used to recover the frequency space from the temporal signal in Fourier NMR. Moreover, the numerical ILT is very consuming in terms of CPU time, thus computing an ILT as proposed by Venkataramanan et al. (17) has only recently become possible. Second, in most cases, spatial exchange and spin evolution cannot be considered separately in relaxation exchange NMR. This situation is very different from what is commonly encountered in Fourier exchange NMR. In the latter case, the slow exchange limit can often be applied during the evolution and detection periods, which allows a straightforward prediction of the cross peak positions. Furthermore, it is precession that is probed during the evolution periods, and this precession can be easily frozen during the mixing time by magnetization storage along the direction of the magnetic field. Consequently, a direct interpretation of the cross-peak intensities as conditional, or exchange, probabilities is often possible in 2D Fourier exchange NMR. It is this relative simplicity that is responsible for this technique's early success.

The interpretation of 2D exchange maps, however, is much less simple. The reason is that the evolution times must be long enough to allow relaxation encoding. To keep matters simple, one would ideally want the exchange rate to be small enough so that exchange would be negligible during the relaxation encoding periods. This limit is called the slow exchange limit. The mixing time, on the other hand, must be long enough so that exchange occurs significantly. The applicability of the slow exchange limit during the evolution period requires that the system relaxes faster than it exchanges. This means relaxation is then necessarily significant during the mixing period, and thus relaxation and exchange must be considered simultaneously at least during the mixing period. Conversely, if the exchange rate was high, while the mixing period was kept short enough to avoid relaxation, significant exchange would occur during the relaxation encoding periods.

In short, the fact that it is relaxation which is probed during the encoding periods implies that exchange can never be restricted to the mixing period and must also be considered during the encoding periods. Consequently, contrary to the case of 2D Fourier exchange spectra, 2D relaxation exchange maps can never be interpreted as pure exchange maps, that is, exchange probability densities. Moreover, relaxation exchange maps are not always symmetric, and often the positions of the peaks are shifted from the cross coordinates of the apparent relaxation rates identified on the diagonal (8). Considering these complications, the aim of this article is

to examine if and how exchange dynamics can be extracted from 2D relaxation exchange maps in the case of multisite exchange.

To address this issue and gain a better understanding about what to expect, 2D relaxation exchange maps were simulated for n -site exchange in the presence of T_2 and T_1 relaxation during the evolution and mixing periods. Following a review of the theory of the evolution of discrete magnetization components under simultaneous relaxation and exchange, the procedure underlying the generation of 2D exchange data sets is recalled. Then, as a first step, results from the literature (2, 8, 23) are illustrated on simulated 1D T_2 data sets to establish that tractable exact analytical solutions can indeed be used to interpret exchange data in the case of two-site exchange. In a second step, it is shown how relaxation and exchange parameters can be extracted from experimental maps of two-site relaxation exchange by comparing experimental and simulated data. As the multisite exchange case is too complex for an analytical treatment, it is shown by simulation that irrespective of ILT artifacts the exchange between three and more relaxation pools may lead to asymmetric 2D exchange maps, whereas two-site 2D exchange maps appear to be always symmetric when square data sets are generated.

II. THEORY OF n -SITE RELAXATION EXCHANGE

Time Evolution

The focus of this treatment is on magnetization components as a function of relaxation rates $R = R^{(1,2)} = 1/T_{1,2}$, where the subscripts 1 and 2 refer to the longitudinal and the transverse relaxation rates, respectively. This notation is sufficiently general to apply to T_1 - T_1 , T_1 - T_2 as well as T_2 - T_2 exchange NMR.

The NMR signal results from the superposition of all the magnetization components

$$s(t) = \sum_i [M_i(t) - M_i^{\text{eq}}]. \quad [1]$$

In the absence of exchange, the evolution of the magnetization component $M_i(t)$ from the relaxation site i follows the differential equation

$$\frac{d}{dt} [M_i(t) - M_i^{\text{eq}}] = -R_i [M_i(t) - M_i^{\text{eq}}], \quad [2]$$

where $R_i = 1/T_1$ and $M_i^{\text{eq}} = M_i^0$ for longitudinal magnetization and $R_i = 1/T_2$ and $M_i^{\text{eq}} = 0$ for transverse

magnetization. When more than one magnetization component are considered, they are collected in a vector, and Eq. [2] becomes

$$\frac{d}{dt} [\mathbf{M}(t) - \mathbf{M}^{\text{eq}}] = -\mathbf{R} [\mathbf{M}(t) - \mathbf{M}^{\text{eq}}], \quad [3]$$

where \mathbf{M} is the vector of magnetization components and \mathbf{R} is a diagonal matrix with the corresponding relaxation rates. This equation has the familiar solution

$$\mathbf{M}(t) - \mathbf{M}^{\text{eq}} = \exp\{-\mathbf{R}(t - t_0)\} [\mathbf{M}(t_0) - \mathbf{M}^{\text{eq}}]. \quad [4]$$

Then, the total NMR signal is given by

$$s(t) = \sum_i [\exp\{-R_i(t - t_0)\} [M_i(t_0) - M_i^{\text{eq}}] + M_i^{\text{eq}}]. \quad [5]$$

Considering that the magnetization components are defined by their relaxation rates, if normalized, they actually stand for the relaxation rate distribution of the system under study. It thus appears that the NMR signal is a discrete form of a Laplace integral equation. In theory, the recovery of the distribution of relaxation rates through a formal ILT is thus possible. In practice, this inversion is highly unstable and is not actually performed in the context of NMR. To obtain the distribution of NMR relaxation rates, the solution of the inverse Laplace problem is not obtained through a formal inversion but numerically approximated. Consequently, it must be understood that what is commonly referred to in the NMR literature as ILTs are in fact nonnegative least square (NNLS) fits using regularization functions or truncated singular value decomposition (SVD). For the sake of clarity, this article adheres to this terminology.

If the magnetization components exchange, an off-diagonal exchange matrix, or kinetic matrix \mathbf{K} , needs to be introduced in Eq. [3], which mixes the magnetization components

$$\frac{d}{dt} [\mathbf{M}(t) - \mathbf{M}^{\text{eq}}] = -(\mathbf{R} + \mathbf{K}) [\mathbf{M}(t) - \mathbf{M}^{\text{eq}}]. \quad [6]$$

Equation [6] still has the familiar solution

$$\mathbf{M}(t) - \mathbf{M}^{\text{eq}} = \exp\{-(\mathbf{R} + \mathbf{K})(t - t_0)\} [\mathbf{M}(t_0) - \mathbf{M}^{\text{eq}}]. \quad [7]$$

The exponential operator can be understood as a time evolution operator, which produces the magnetization state at time t given the magnetization state at time t_0 .

The time evolution operator is evaluated by diagonalizing the matrix sum $\mathbf{R} + \mathbf{K}$ with the help of the rotation matrix \mathbf{Q} ,

$$\mathbf{U}(t - t_0) = \mathbf{Q} \exp\{-\mathbf{Q}^{-1}(\mathbf{R} + \mathbf{K})\mathbf{Q}(t - t_0)\}\mathbf{Q}^{-1}. \quad [8]$$

Content of the Kinetic Matrix

Considering a three-site exchange as an example, the kinetic matrix \mathbf{K} can be written as

$$\mathbf{K} = \begin{bmatrix} k_{11} & -k_{12} & -k_{13} \\ -k_{21} & k_{22} & -k_{23} \\ -k_{31} & -k_{32} & k_{33} \end{bmatrix}, \quad [9]$$

where k_{ij} is the exchange rate between site i and site j . As \mathbf{K} only mixes magnetization components and preserves the total magnetization, detailed mass balance requires that whatever amount of magnetization is lost in one component has to be recovered from other components, i.e.:

$$\mathbf{K} \mathbf{M}^{\text{eq}} = 0. \quad [10]$$

For example, for magnetization component M_1 , we can write

$$k_{11} M_1^{\text{eq}} - k_{12} M_2^{\text{eq}} - k_{13} M_3^{\text{eq}} = 0. \quad [11]$$

Similarly, whatever total amount of magnetization is received by one of the magnetization components from other magnetization components has to be restored to them. For example, for magnetization component M_1 ,

$$k_{12} M_2^{\text{eq}} + k_{13} M_3^{\text{eq}} = k_{21} M_1^{\text{eq}} + k_{31} M_1^{\text{eq}}. \quad [12]$$

This, with the help of the previous equation, leads to

$$k_{11} - k_{21} - k_{31} = 0, \quad [13]$$

so that the column sums of \mathbf{K} vanish.

By applying the mass balance to each of the three components, six equations are obtained. Furthermore, the total amount of magnetization exchanged is necessarily conserved. Consequently, of the initial nine parameters k_{ij} , only four remain independent. In the general case of n -site exchange, the kinetic matrix is determined by $(n - 1)^2$ independent parameters.

Note that the rates k_{ij} apply to the forward kinetics from state i to state j , so that the rates k_{ji} apply to the reverse kinetics from state j to state i . The associated

equilibrium constant K_{ij} , which is defined by the ratio $[M_j]/[M_i]$ of concentrations, is given by

$$K_{ij} = \frac{[M_j]}{[M_i]} = \frac{k_{ij}}{k_{ji}}. \quad [14]$$

FID in Response to a Single Excitation Pulse

Given the state of the magnetization at time t_0 after an excitation pulse, the transverse magnetization at time t_1 later is given by Eq. [7]

$$\mathbf{M}(t_1 + t_0) = \exp\{-[\mathbf{R}^{(2)} + \mathbf{K}](t_1 + t_0)\}\mathbf{M}(t_0). \quad [15]$$

The apparent formal simplicity of this equation is misleading. As we are dealing with an exponential function of a nondiagonal matrix, the prediction of the decay of the total transverse magnetization is not trivial. It involves the determination of the eigenvalues and eigenvectors of the exponential operator as formally stated in Eq. [8], a task which can be performed analytically only if the number of sites i remains limited and is not possible when dealing with unknown continuous distributions of sites.

General Analytical Solutions for Two-Site Exchange

For reference, the general solution of Eq. [6] for two-site exchange is recalled (23, 24). As there are only two sites, the magnetization vector can be written explicitly as

$$\mathbf{M} = \begin{bmatrix} M_a \\ M_b \end{bmatrix}, \quad [16]$$

and the kinetic matrix can be written upon balancing the magnetization as

$$\mathbf{K} = \begin{bmatrix} k_a & -k_b \\ -k_a & k_b \end{bmatrix}, \quad [17]$$

where $k_b = k_{ab}$ and $k_a = k_{ba} M_b/M_a$. Consequently, the matrix $\mathbf{R} + \mathbf{K}$ can be written as

$$\mathbf{R} + \mathbf{K} = \begin{bmatrix} R_a^{(1,2)} + k_a & -k_b \\ -k_a & R_b^{(1,2)} + k_b \end{bmatrix}. \quad [18]$$

The eigenvalues λ_+ and λ_- of this matrix are given by (23)

$$\lambda_+^{1,2} = \frac{(R_a^{1,2} + R_b^{1,2} + k_a + k_b) + \sqrt{(R_b^{1,2} + k_b - R_a^{1,2} - k_a)^2 + 4k_a k_b}}{2}, \quad [19a]$$

$$\lambda_-^{1,2} = \frac{-(R_a^{1,2} + R_b^{1,2} + k_a + k_b) - \sqrt{(R_b^{1,2} + k_b - R_a^{1,2} - k_a)^2 + 4k_a k_b}}{2}. \quad [19b]$$

The rotation matrix \mathbf{Q} can be deduced from the eigenvectors, allowing the calculation from Eqs. [7] and [8] of the exponential of the $\mathbf{R} + \mathbf{K}$ matrix, that is of the evolution operator of the magnetization. Experimentally, the eigenvalues of the $\mathbf{R} + \mathbf{K}$ matrix are the coordinates of the peaks of the distribution of the exponential decay rates obtained by the numerical approximate of the solution of the inverse Laplace problem (the so-called “ILT,” as explained in the section “time evolution”). As expected, these coordinates tend toward the relaxation rates when the exchange rates become negligibly small compared to the relaxation rates. This is the slow exchange limit discussed in the preceding section. The intensities of the peaks can be obtained analytically from the rotation matrix \mathbf{Q} in Eq. [8]. Their complicated expressions need not be reproduced here but can be found in the literature (23). They correspond to the magnetization values only in the slow exchange limit.

Evolution Magnetization in T_2 - T_2 Exchange NMR

As an example, the time evolution of the magnetization is examined for a T_2 - T_2 exchange experiment with a mixing period during which the magnetization is stored along the direction of the magnetic field and experiences a T_1 relaxation (Fig. 1).

The magnetization after the mixing time t_m follows from Eq. [7],

$$\begin{aligned} \mathbf{M}(t_m + t_1 + t_0) - \mathbf{M}^0 \\ = \exp\{-[\mathbf{R}^{(1)} + \mathbf{K}](t_m)\}(\mathbf{M}(t_1 + t_0) - \mathbf{M}^0). \end{aligned} \quad [20]$$

During the evolution period t_1 and the detection period t_2 , the magnetization is given by

$$\mathbf{M}(t_1 + t_0) = \exp\{-[\mathbf{R}^{(2)} + \mathbf{K}](t_1 + t_0)\}\mathbf{M}(t_0) \quad [21]$$

and

$$\begin{aligned} \mathbf{M}(t_2 + t_m + t_1 + t_0) \\ = \exp\{-[\mathbf{R}^{(2)} + \mathbf{K}](t_2)\}\mathbf{M}(t_m + t_1 + t_0). \end{aligned} \quad [22]$$

The last three equations combine into

$$\begin{aligned} \mathbf{M}(t_2 + t_m + t_1 + t_0) \\ = \exp\{-[\mathbf{R}^{(2)} + \mathbf{K}](t_2)\}\{\exp\{-[\mathbf{R}^{(1)} + \mathbf{K}](t_m)\} \\ \times (\exp\{-[\mathbf{R}^{(2)} + \mathbf{K}](t_1 + t_0)\}\mathbf{M}(t_0) - \mathbf{M}^0) + \mathbf{M}^0\}. \end{aligned} \quad [23]$$

Statistical Interpretation of Peak Intensities in the Slow Exchange Limit

In 2D Fourier exchange NMR experiments, the fast exchange limit may apply during the mixing time so that relaxation can be neglected during t_m , whereas the slow exchange limit applies during the evolution and detection times. This situation is never encountered in 2D relaxation exchange NMR. Only the following three cases may be encountered. Their corresponding evolution operators are given in Table 1.

1. The exchange is slow during the evolution periods, which means that the time scale of exchange is long compared to the time scale of relaxation, and pure relaxation encoding is possible during the evolution periods. Consequently, there is no fast exchange during the mixing period.
2. The exchange is fast compared to relaxation. Then, the fast exchange limit is satisfied during the mixing time. In this case, the mixing period involves only exchange but not relaxation, whereas the evolution and detection periods encode both, relaxation and exchange.
3. The exchange rate is commensurate with the relaxation rates, and both must be considered during the evolution, mixing, and detection periods.

Only in the first case can the 2D relaxation cross peaks be analyzed in terms of exchange kinetics, although not in a simple manner. Being in the slow exchange limit during evolution means that one can measure the relaxation rate R_i at time t and identify it

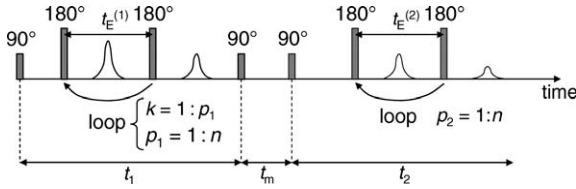


Figure 1 Pulse sequence for a T_2 - T_2 exchange experiment. Following a $\pi/2$ read pulse at time t_0 , a CPMG sequence of p_1 π pulses equally spaced by $t_E^{(1)}$ is applied during a first evolution period t_1 . The transverse magnetization is encoded according to T_2 during t_1 . It is then stored along the direction of the magnetic field with the help of a $\pi/2$ pulse where it subsequently relaxes with T_1 during the mixing time t_m . After the mixing time, a $\pi/2$ read pulse returns the magnetization to the transverse plane, and its T_2 decay is followed for a second time in the detection period t_2 by recording the amplitude of each echo from a second CPMG sequence of n π pulses equally spaced by $t_E^{(2)}$. This sequence is repeated varying p_2 between 1 and n , resulting in an n^2 time-domain matrix. After ILT, one obtains a 2D T_2 - T_2 correlation map.

with the magnetization of the corresponding site M_i . In this case, the slow exchange limit applies to the t_1 and t_2 encoding periods, and Eq. [23] simplifies to

$$\begin{aligned} \mathbf{M}(t_2 + t_m + t_1 + t_0) &= \exp\{-[\mathbf{R}^{(2)} t_2]\} \exp\{-[\mathbf{R}^{(1)} + \mathbf{K}](t_m)\} \\ &\times (\exp\{-\mathbf{R}^{(2)}(t_1 + t_0)\} \mathbf{M}(t_0) - \mathbf{M}^0) + \mathbf{M}^0. \end{aligned} \quad [24]$$

As the relaxation matrix $\mathbf{R}^{(2)}$ is diagonal, the magnetization of a particular site i at the end of the evolution period is obtained as

$$\begin{aligned} M_i(t_1 + t_0) &\sim \exp\{-R_i^{(2)} t_1\} M_i(t_0) \\ &= \exp\{-t_1/T_{2,i}\} M_i(t_0). \end{aligned} \quad [25]$$

After the mixing time t_m , one obtains from Eq. [7],

$$\begin{aligned} M_j(t_m + t_1 + t_0) - M_j^0 &= \sum_i \{[\exp\{-[\mathbf{R}^{(1)} + \mathbf{K}]t_m\}]_{ji} (M_i(t_1 + t_0) - M_i^0)\}, \\ & \quad [26] \end{aligned}$$

while similarly to what occurred during the evolution period t_1 , only T_2 is encoded during the detection period t_2 ,

$$\begin{aligned} M_j(t_2 + t_m + t_1 + t_0) &\sim \exp\{-R_j^{(2)} t_2\} M_j(t_m + t_1 + t_0) \\ &= \exp\{-t_2/T_{2,j}\} M_j(t_m + t_1 + t_0). \end{aligned} \quad [27]$$

The resultant time-domain signal is then approximated by

$$\begin{aligned} M_j(t_2 + t_m + t_1 + t_0) &\sim \exp\{-t_2/T_{2,j}\} \\ &\times \left[\sum_i \{[\exp\{-[\mathbf{R}^{(1)} + \mathbf{K}]t_m\}]_{ji} \right] \\ &\times (\exp\{-t_2/T_{2,i}\} M_i(t_0) - M_i^0) + M_j^0. \end{aligned} \quad [28]$$

It is apparent that after 2D inversion over t_1 and t_2 , cross peaks arise at coordinates (T_{2i}, T_{2j}) with amplitudes given by

$$M_{ij} = [\exp\{-[\mathbf{R}^{(1)} + \mathbf{K}]t_m\}]_{ji} M_i(t_0). \quad [29]$$

Therefore, when this slow exchange limit is fulfilled for the encoding and detection periods t_1 and t_2 , the cross-peak amplitude represents the magnetization from site j that originated from site i before the mixing time t_m .

For the sake of understanding, the virtual case of fast exchange during the mixing is considered. Then, we would have

$$\exp\{-[\mathbf{R}^{(1)} + \mathbf{K}]t_m\} \sim \exp\{-\mathbf{K}t_m\}. \quad [30]$$

In this limit, magnetization would have been conserved during the exchange and thus, upon normalization, could have been assigned to the probability of site occupancy. The cross peaks would then have mapped the joint probability of molecules or spins being at site j at time $t_0 + t_1 + t_m \sim t_0 + t_m$ and at site i at time $t_0 + t_1 \sim t_0$. This joint probability density can be expressed in terms of the conditional

Table 1 Evolution Operators of the Three Cases That May Occur in 2D Relaxation Exchange NMR as Described in the Text

	$U(t_1)$	$U(t_m)$	$U(t_2)$
Case (1)	$\exp\{-[\mathbf{R}](t_1)\}$	$\exp\{-[\mathbf{R} + \mathbf{K}](t_m)\}$	$\exp\{-[\mathbf{R}](t_2)\}$
Case (2)	$\exp\{-[\mathbf{R} + \mathbf{K}](t_1)\}$	$\exp\{-[\mathbf{K}](t_m)\}$	$\exp\{-[\mathbf{R} + \mathbf{K}](t_2)\}$
Case (3)	$\exp\{-[\mathbf{R} + \mathbf{K}](t_1)\}$	$\exp\{-[\mathbf{R} + \mathbf{K}](t_m)\}$	$\exp\{-[\mathbf{R} + \mathbf{K}](t_2)\}$

The time periods t_1 , t_m , and t_2 are defined in Fig. 1. For the T_2 - T_2 exchange experiment schematized in Fig. 1, \mathbf{R} stands for $\mathbf{R}^{(1)}$ during t_m and for $\mathbf{R}^{(2)}$ during t_1 and t_2 .

probability density of a spin being at site j knowing it started at time i following

$$M_{ji}(t_0 + t_m) = \langle R_j, (t_0 + t_m) | R_i, t_0 \rangle_{ji} M_i(t_0). \quad [31]$$

Consequently, comparing Eqs. [27] and [29], the exponential exchange operator could have been identified with the conditional probability matrix

$$\exp\{-\mathbf{K} t_m\} = \left[\langle R_j, (t_0 + t_m) | R_i, t_0 \rangle_{ji} \right], \quad [32]$$

and the cross-peak intensities would have directly mapped the elements of the exponential of the kinetic matrix, or equivalently of the conditional probability, as

$$\begin{aligned} M_{ji}(t_0 + t_m) &= \langle R_j, (t_0 + t_m) | R_i, t_0 \rangle_{ji} M_j(t_0) \\ &= [\exp\{-\mathbf{K} t_m\}]_{ji} M_i(t_0). \end{aligned} \quad [33]$$

This means that the evolution of the intensities of the peaks with the length of the mixing period would have decayed according to the eigenvalues of the exchange matrix.

However, in reality, the fast exchange limit cannot be fulfilled during the mixing time when the slow exchange limit applies during the encoding times. As a result, magnetization is not conserved during the mixing time because of relaxation. Nevertheless, if all the sites had the same relaxation rate R_{all} , one could still write

$$\begin{aligned} &[\exp\{-(\mathbf{R}^1 + \mathbf{K}) t_m\}]_{ji} \\ &= \exp(-R_{\text{all}} t_m) [\exp\{-\mathbf{K} t_m\}]_{ji} \\ &= \exp(-t_m/T_{1,\text{all}}) [\exp\{-\mathbf{K} t_m\}]_{ji}, \end{aligned} \quad [34]$$

and the cross-peaks intensities would still be a representation of the elements of the kinetic matrix albeit weighted by relaxation during the mixing time

$$\begin{aligned} M_{ji}(t_0 + t_m) &= \exp(-R_{\text{all}} t_m) \langle R_j, (t_0 + t_m) | R_i, t_0 \rangle_{ji} M_i(t_0) \\ &= \exp(-R_{\text{all}} t_m) [\exp\{-\mathbf{K} t_m\}]_{ji} M_i(t_0). \end{aligned} \quad [35]$$

Nevertheless, 2D relaxation exchange NMR is of interest only when the sites relax differently, so that the case above is not pertinent. In general, even in the slow exchange limit, one cannot go further other than writing

$$\begin{aligned} M_{ji}(t_0 + t_m) &= [\exp\{-(\mathbf{R}^{(1)} + \mathbf{K}) t_m\}]_{ji} M_i(t_0) \\ &= [\mathbf{Q} \exp\{-\mathbf{Q}^{-1}(\mathbf{R}^1 + \mathbf{K})\mathbf{Q} t_m\} \mathbf{Q}^{-1}]_{ji} M_i(t_0). \end{aligned} \quad [36]$$

The other two cases (as explained at the beginning of this section, namely exchange compared to relaxation and exchange commensurate with relaxation) are even more complex as magnetization is not conserved or follows multiple single relaxation paths. The evolution of magnetization must be predicted working back from the general Eqs. [8] and [23]. As a consequence, 2D relaxation exchange maps cannot be interpreted in terms of conditional probability densities, and the observed decay rates are not associated with single-site relaxation rates (8, 23).

Multisite Relaxation Exchange

In the case of an interconnected system of more than two sites, tracking the general analytical expression of the rotation matrix \mathbf{Q} to diagonalize the evolution operator becomes extremely tedious at best and close to impracticable in most cases. Furthermore, as the slow exchange limit is typically violated in relaxation exchange NMR, 2D exchange maps cannot simply be interpreted in terms of joint probability densities. At this stage of the discussion, as no obvious generalizations can be made from the two-site analytical solution, it becomes clear that only numerical simulations that take relaxation and exchange into account at all time periods of the 2D exchange experiment can support the interpretation of the experimental data.

III. NUMERICAL SIMULATIONS

The simulation procedure provides the opportunity to generate time-domain exchange data sets free of experimental noise, which can be processed by one of the available so-called ILT algorithms to evaluate methods of extracting relaxation, exchange, and population parameters from the exchange maps. Given a chosen set of \mathbf{K} , $\mathbf{R}^{(2)}$, and $\mathbf{R}^{(1)}$ matrices and an initial magnetization vector $\mathbf{M}(t_0)$, which typically is proportional to the population of sites, the magnetization vector $\mathbf{M}(t_1 + t_0)$ is calculated according to Eq. [21] for each site i and at each time $t_1 = p_1 t_E^{(1)}$ with p_1 varying between 1 and n :

$$\begin{aligned} M_i(t_1 + t_0) &= M_i(p_1 t_E^{(1)} + t_0) \\ &= \sum_{j=1}^n ([\exp\{-(\mathbf{R}^{(2)} + \mathbf{K})(p_1 t_E^{(1)})\}]_{ji} M_j(t_0)). \end{aligned} \quad [37]$$

This provides a 1D time-domain data set for each site. Then, for each value of p_1 the magnetization vector $\mathbf{M}(t_2 + t_m + p_1 t_E^{(1)} + t_0)$ is calculated according to

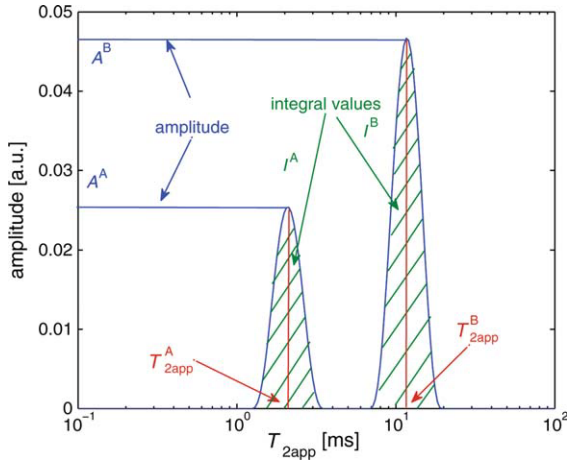


Figure 2 Notation for 1D relaxation time distributions of two exchanging sites. [Color figure can be viewed in the online issue, which is available at www.interscience.wiley.com.]

Eq. [23] for each site j and at each time $t_2 = p_2 t_E^{(2)}$ with p_2 running from 1 to n . Thus, for each site j , an individual n^2 2D data set is obtained in the time domain,

$$M_j(t_2 + t_m + t_1 + t_0) = M_j(p_2 t_E^{(2)} + t_m + p_1 t_E^{(1)} + t_0) \\ = \sum_{r=1}^n \{ [\exp\{-(\mathbf{R}^{(2)} + \mathbf{K})p_2 t_E^{(2)}\}]_{jr} \sum_{i=1}^n ([\exp\{-(\mathbf{R}^{(1)} + \mathbf{K})t_m\}]_{ri} (M_i(p_1 t_E^{(1)}) - M_i^0) + M_r^0) \}. \quad [38]$$

Finally, the simulated 2D data set is the sum of the individual 2D data sets for each site j ,

$$S(t_1, t_m, t_2) = S(p_2 t_E^{(2)}, t_m, p_1 t_E^{(1)}) \\ = \sum_{j=1}^n M_j(p_2 t_E^{(2)}, t_m, p_1 t_E^{(1)}). \quad [39]$$

This 2D time-domain array simulates the data from the 2D relaxation exchange NMR experiment (Fig. 3) (16). Finally, the 2D T_2 - T_2 exchange map is obtained by 2D ILT of this array. The numerical approximation of the inversion, commonly called ILT, is performed with a software developed by the group of Prof. P. Callaghan and based on the method published by Venkataramanan (namely a NNLS fit using SVD) (17, 20, 25, 26).

Procedure for 1D Simulations

As a preparatory check for 2D exchange data simulations, and to gain prior insight into relaxation exchange NMR, 1D CPMG data are analyzed. Time-domain data sets were generated for two-site exchange using Eq. [39]

$$S_{1D}^{\text{two sites}}(t_1, t_m, t_2) = S_{1D}^{\text{two sites}}(p_2 t_E^{(2)}, t_m, p_1 t_E^{(1)}) \\ = M_A(p_2 t_E^{(2)}, t_m, p_1 t_E^{(1)}) + M_B(p_2 t_E^{(2)}, t_m, p_1 t_E^{(1)}) \quad [40]$$

and subsequently converted into distributions of relaxation times by ILT. The notation used in Eq. [38] is the following (Fig. 2):

- T_{2app}^A and T_{2app}^B denote the coordinates of the peaks on a transverse relaxation times scale obtained by ILT of the simulated data.
- A^A and A^B denote the amplitudes of the peaks in the relaxation time distribution of peaks A and B, respectively, calculated from the simulated data by ILT.
- I_A and I_B denote the areas of the ILT peaks of sites A and B, respectively.

The input parameters chosen for the 1D simulations are summarized in Table 2. The exchange time, e.g., the inverse of the exchange rate, is varied between 0.01 and 500 ms. For these parameters, 1D relaxation decays were simulated and inverted by ILT to extract the T_{2app} coordinates of the peaks in the relaxation time distributions, the peak amplitudes, and the peak integrals. The results are summarized graphically in Figs. 3(a,b).

To check for a possible influence of the sampling interval t_E on the output results, two sampling rates commensurate with the used exchange time were tested, namely $t_E = 0.1$ and 0.01 ms. The simulations led to the same results in both cases. The data presented here correspond to $t_E = 0.1$ ms.

Results of 1D Simulations

The influence of the exchange rate on the peak integrals and peak positions is illustrated in Figs. 3 and 4. When the exchange time becomes short compared to the relaxation times, one of the peaks grows at the expense of the other. For an exchange time lower than 1 ms, only a single peak is observed, and the peak integral corresponds to the number of spins from both sites [Fig. 3(b)]. On the other hand, when the exchange time is at least 10 times longer than the

Table 2 Input Parameters for Simulations of 1D T_2 Distributions

Parameter	Value
T_2^A	2.5 ms
T_2^B	25 ms
A^A	0.5
A^B	0.5

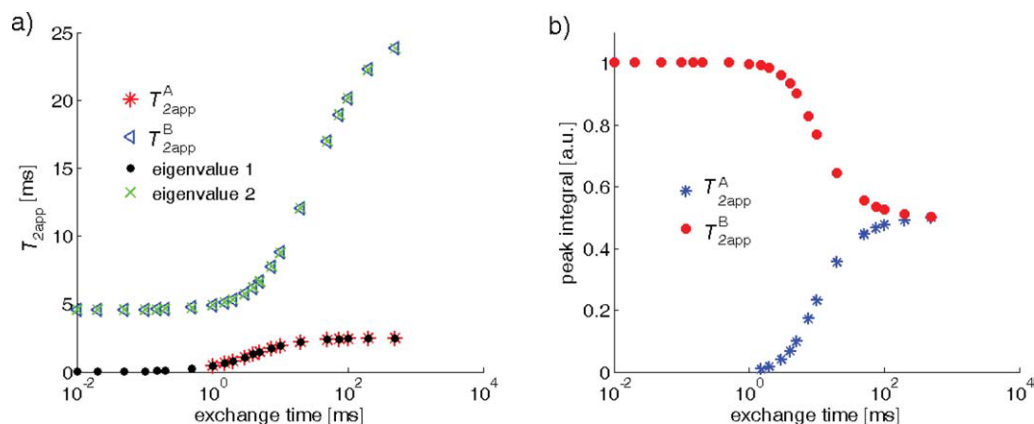


Figure 3 Results of 1D simulations for two-site exchange. (a) Apparent relaxation times derived from relaxation time distributions and eigenvalues of the $\mathbf{R} + \mathbf{K}$ matrix. (b) Peak integrals of relaxation time distributions. [Color figure can be viewed in the online issue, which is available at www.interscience.wiley.com.]

longest relaxation time, the peak integrals provide the correct population values. For shorter exchange times, the population of the peak with the longer relaxation time is overestimated and that of the other is underestimated. This observation is in line with the analytical predictions (2, 23).

To verify that these results were not an artifact of the ILT algorithm, the simulated relaxation curves were fitted with two exponential decay functions. The fit results confirmed that the peak integrals of the relaxation time distributions correspond to the amplitudes of the exponential fit functions. The amplitudes follow exactly the same pattern as the peak integrals, validat-

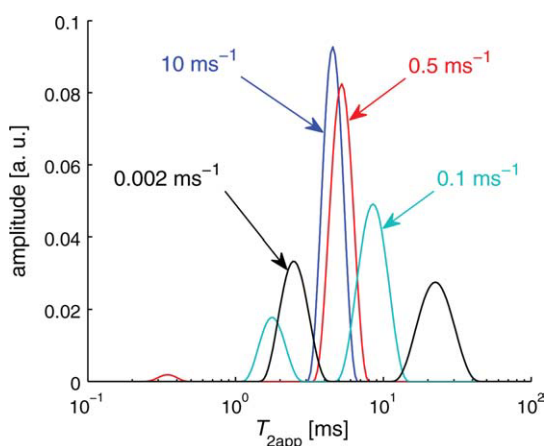


Figure 4 Examples of 1D spectra of two-site exchange for fast exchange ($k = 10 \text{ ms}^{-1}$), two intermediate exchanges ($k = 0.5$ and 0.1 ms^{-1}), and slow exchange ($k = 0.002 \text{ ms}^{-1}$). [Color figure can be viewed in the online issue, which is available at www.interscience.wiley.com.]

ing the use of peak integrals in the analysis of relaxation-time distributions to quantify spin populations.

It is emphasized that the relaxation times extracted from the maxima of the relaxation time distributions are apparent relaxation times, corresponding to the eigenvalues of the sum of the exchange and relaxation matrices and as such are strongly affected by the exchange rate (Fig. 4). An exchange time 100 times longer than the longest T_2 component is required to obtain an unbiased estimate of T_2 . Shorter exchange times lower the apparent transverse relaxation times. When the exchange approaches infinity, the shorter apparent T_2 value tends toward zero, whereas the longer one shifts toward a value corresponding to the population-weighted average of the relaxation rates, namely slightly below 5 ms in the present case.

In the intermediate exchange region between the fast and the slow exchange limits, the apparent relaxation times T_{2app} follows the eigenvalues of the $\mathbf{R} + \mathbf{K}$ matrix [Fig. 3(a)]. The excellent agreement between the eigenvalues and the apparent relaxation times shows that, as expected from Eq. [6], the apparent relaxation times are indeed given by the eigenvalues of the $\mathbf{R} + \mathbf{K}$ matrix. To anticipate the discussion on 2D exchange experiments, we note that a 1D relaxation time distribution can be understood in terms of a projection of a 2D distribution onto one axis, and thus that the peaks in 2D distributions will be shifted by exchange along the relaxation-time axis in the same way as those in 1D distributions.

The results reported so far have all been simulated with one set of T_2 values, i.e., with $T_2^A = 2.5 \text{ ms}$ and $T_2^B = 25 \text{ ms}$. Similar results were obtained with other choices of relaxation times as input variables.

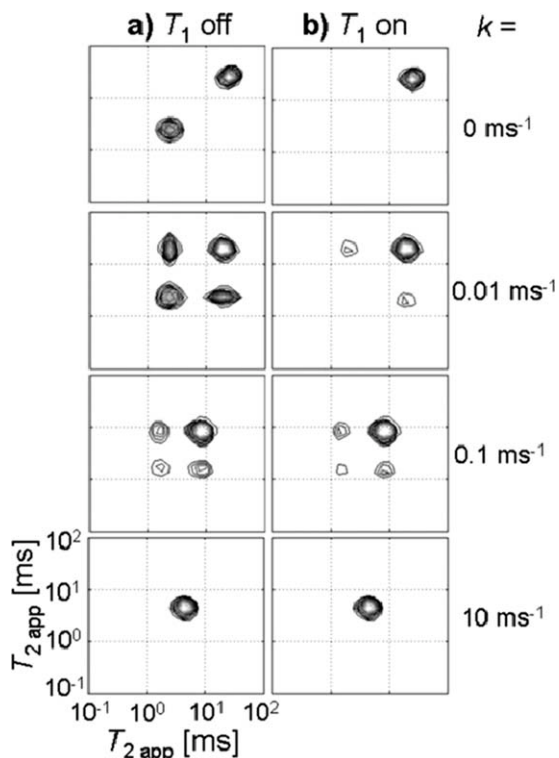


Figure 5 2D distributions for two-site exchange simulated with the parameters of Table 3 with different exchange rates in the limit of infinite longitudinal relaxation times (a) and with longitudinal relaxation times equal to six times the transverse relaxation times (b).

The dependences of the amplitudes and apparent relaxation times on the exchange time are similar in all cases, which corroborates the conclusions derived above. Moreover, if T_2 is replaced by T_1 , the results of this study do not change. The T_1 values are affected by the exchange in the same way as the T_2 values.

2D Simulations: Two-Site Exchange

The time-domain data for two-site exchange were transformed to 2D exchange maps (Fig. 5) by 2D ILT. The 2D distributions exhibit two diagonal peaks and two off-diagonal peaks, which reveal the exchange between the two sites.

Depending on the exchange time and the exchange rate, one diagonal peak is observed for fast exchange, two diagonal peaks for slow exchange, and additional cross peaks for intermediate exchange. As relaxation during the mixing period complicates the analysis of peak integrals (see Eq. [23]), simulations with the longitudinal relaxation time on (T_1 finite) and off (T_1 infinite) are compared. Simulations performed in this way with the parameters specified in Table 3 produced the exchange maps of Fig. 5.

The mixing time was set equal to the exchange time in each case except in the first case (top).

When the exchange is very fast (top left), the exchange map exhibits a single peak in accordance with the 1D study. When the exchange time is increased and becomes comparable to the relaxation times, cross peaks appear as well as two distinct diagonal peaks (top right, bottom left). When the exchange time becomes long, i.e., about 10 times the longest value of T_2 , the exchange is too slow to be seen and the cross peaks disappear (bottom right).

The peak intensities corresponding to the peak integrals in the 2D maps vary with the mixing time t_m . The diagonal peaks decay (Fig. 6, top) and the cross peaks initially grow exponentially with the mixing time t_m (Fig. 6, bottom). This has been simulated for two-site exchange with $T_2 = 1$ ms and 10 ms for the two sites (Fig. 6). Without relaxation during the mixing time, the cross-peak intensity grows exponentially toward a dynamic equilibrium value (Fig. 6, bottom left). The time constants of the cross-peak build-up were determined via exponential fits. They are found to correspond to the inverse of the nonzero eigenvalue of the exchange matrix \mathbf{K} , i.e., to the input parameters $1/k_1 = 50$ ms and $1/k_2 = 100$ ms used in the simulations. As longitudinal relaxation has been turned off in the simulation, any change of peak intensity can indeed only be due to the exchange, so that the peak intensities can only change by mixing between the two populations.

When longitudinal relaxation is included during the mixing time t_m , the cross-peak intensity goes to zero for long mixing times (Fig. 6, bottom right), and only when the longitudinal relaxation times are of the order of the exchange time and much larger than the transverse relaxation times did the cross peaks become intense. The build-up of the cross-peak intensity is no longer determined by the nonzero eigenvalue of the exchange matrix \mathbf{K} , as its growth is now affected by the T_1 relaxation of both sites.

Table 3 Parameters Used to Produce the Exchange Maps of Fig. 7

Parameter	Value
T_2^A	2.5 ms
T_2^B	25 ms
T_1^A	Infinite, 15 ms
T_1^B	Infinite, 150 ms
k_1	10 ms^{-1}
k_2	0.1 ms^{-1}
k_3	0.01 ms^{-1}
k_4	0 ms^{-1}

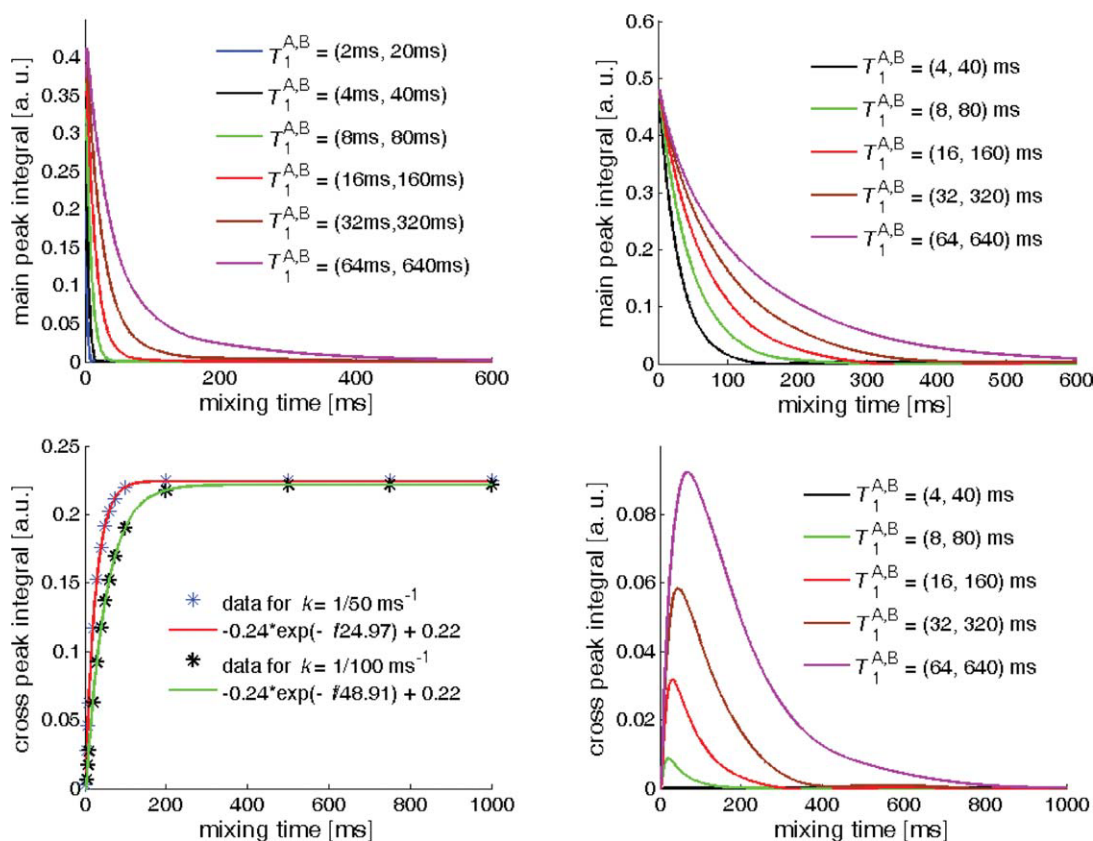


Figure 6 Evolution of peak integrals with the mixing time t_m in 2D maps for two-site exchange. Top: Integrals of the diagonal peaks with the short (left) and the long (right) relaxation time with T_1 relaxation during the mixing time. Bottom: integral of cross peaks without (left) and with (left) longitudinal relaxation during the mixing time. The cross-peak build-up shown on the bottom left was simulated for two exchange times $1/k_1 = 50$ ms and $1/k_2 = 100$ ms. The exchange time for the curves on the bottom right is $1/k_2 = 100$ ms. [Color figure can be viewed in the online issue, which is available at www.interscience.wiley.com.]

2D Simulations: Three-Site Exchange

The results obtained for two-site exchange simulations did follow the known analytical solutions recalled in section “general analytical solutions for two-site exchange” (2, 8, 23). To date, there is no published analytical solution for the case of relaxation and exchange between more than two sites. However, this case can be modeled with Eq. [23]. There is a fundamental difference between two- and n -site exchanges. For two sites, the exchange maps are symmetric (if both dimensions are acquired with the same evolution times) as mass balance requires the forward and backward exchange to be identical. When exchange takes place between more than two sites, detailed mass balance applies to the overall exchange but not to subsets consisting of only two of the n sites, so that asymmetric exchange maps can arise. Figure 7 shows two simulated maps for three-site exchange, one symmetric (left) and the other one not (right). To obtain a symmetric map, all

exchange times have to have the same value, whereas they differ strongly in the nonsymmetric case.

2D Simulations: Noise and Baseline Artifacts

A further source of asymmetry in experimental data sets can be linked to the sensitivity of the numerical method used to approximate the inverse Laplace problem (the ILT algorithm) to noise and baseline artifacts (23). To prove this point, a constant baseline and zero-mean Gaussian white noise with a standard deviation equal to a percentage of the maximum value in the simulated 2D data sets without any noise were added to the simulated data. The corresponding exchange maps derived by 2D ILT were analyzed for the peak integrals and the peak coordinates in the T_2 – T_2 space (Fig. 8). Figure 8(a) quantifies the effect of the noise on the peak integrals. The amplitude of the

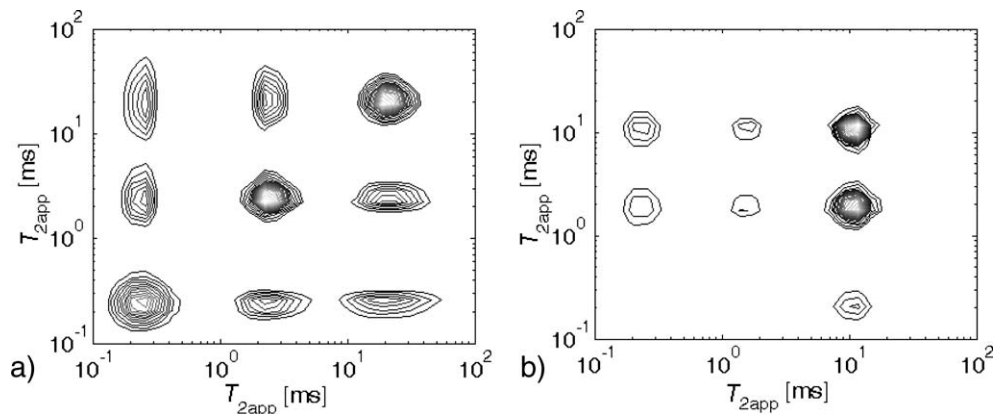


Figure 7 2D maps for three-site exchange. (a) Symmetric map with $k_{12} = k_{13} = k_{23} = k_{32} = 250$ ms. (b) Asymmetric map with $k_{12} = 400$ ms, $k_{13} = 20$ ms, $k_{23} = 3000$ ms, and $k_{32} = 10$ ms. The longitudinal relaxation times were set to four times the corresponding transverse relaxation times.

noise strongly affects the value of the integrals. As the peak integrals also depend on both the exchange rate and the longitudinal relaxation times, the accuracy with which exchange rates and longitudinal

relaxation times can be determined is affected by the noise. The peak positions can also be shifted on the T_2 - T_2 map in the presence of noise [Fig. 8(b)]. This effect is not negligible as, remarkably, one of the di-

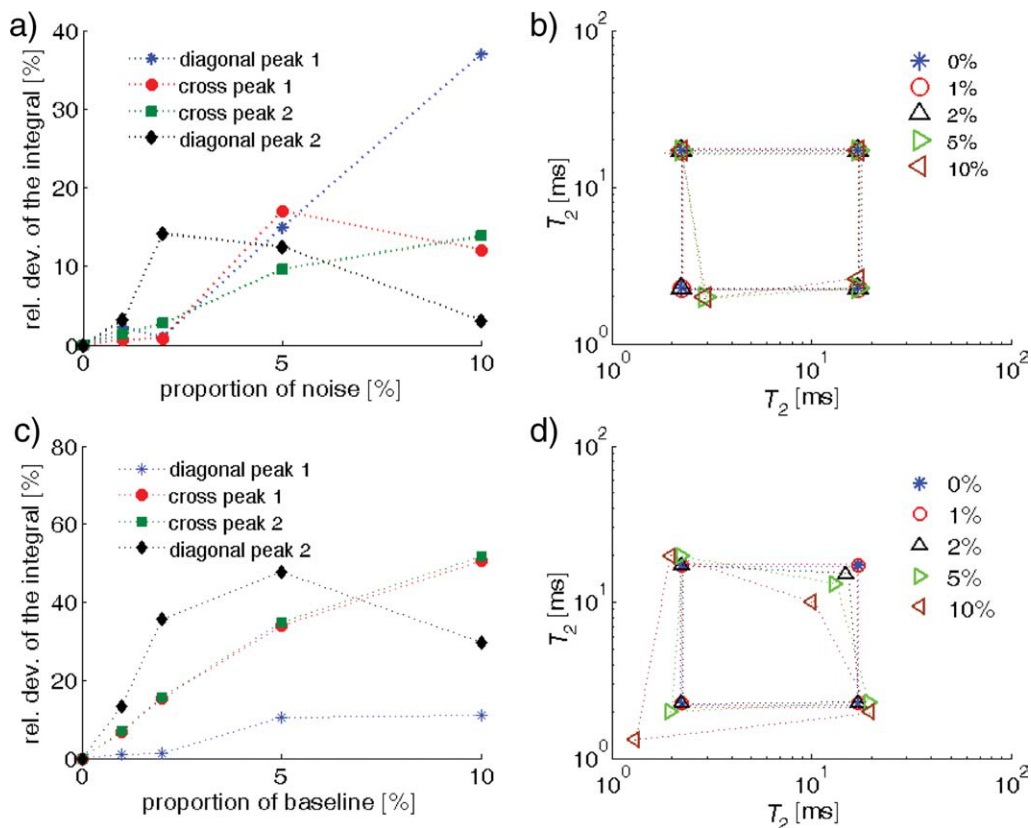


Figure 8 Effects of the noise (a and b) and baseline offset (c and d) on the peak intensities (a and c) and peak coordinates (b and d). The relative deviation of the integrals from the value in the absence of noise is given in percent. The baseline offset is specified relative to the maximum value of the original time-domain 2D data set. [Color figure can be viewed in the online issue, which is available at www.interscience.wiley.com.]

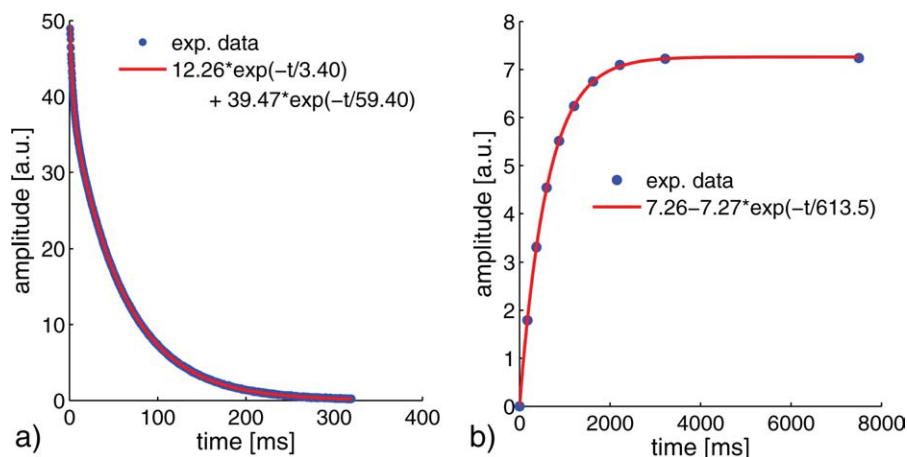


Figure 9 Water saturating silica particles. (a) Transverse magnetization decay. (b) Longitudinal magnetization build-up measurements of water saturating silica particles. [Color figure can be viewed in the online issue, which is available at www.interscience.wiley.com.]

agonal peaks shifts away from the diagonal when the noise level is only just above 2%.

Nonzero baselines also produce similarly strong artifacts in the peak intensities (c) and the peak positions (d). As shown in Figs. 8(c,d), a baseline offset of 2% is sufficient to produce distorted exchange maps.

IV. COMPARISON WITH EXPERIMENTS

The formalism to simulate 2D relaxation exchange maps was tested by modeling experimental maps for two-site exchange to extract relaxation and exchange parameters. Silica particles were synthesized according to the Stöber reaction (27) as this procedure is known to yield monodisperse particles, which are good candidates for simple two-site exchange when

saturated with water. The two relaxation sites are expected to be the bulk water in the interstitial space of the closely packed structure on the one hand, and the water on the surface and within the micropores of the silica particles on the other hand. For the particle synthesis, 60 mL of tetraethoxysilane, 405 mL of NH_3 at 25% in solution, and 1.5 L of ethanol were mixed together. Then, the particles were washed first with ethanol and a second time with water, and their size was determined with a scanning electronic microscope to be 500 nm with a standard deviation of 40 nm.

Figure 9 depicts the transverse (a) and longitudinal magnetization build-up (b) curves measured by the CPMG sequence and the saturation recovery method, respectively. As expected, the system exhibits two apparent transverse relaxation times T_2 , which correspond to two different sites, but only a single apparent relaxation time T_1 . Considering the results obtained in the 1D simulations (see section “procedure for 1D simulations”), we can conclude from the observation of a single T_1 that the exchange time is small compared to the spin-lattice relaxation time. In

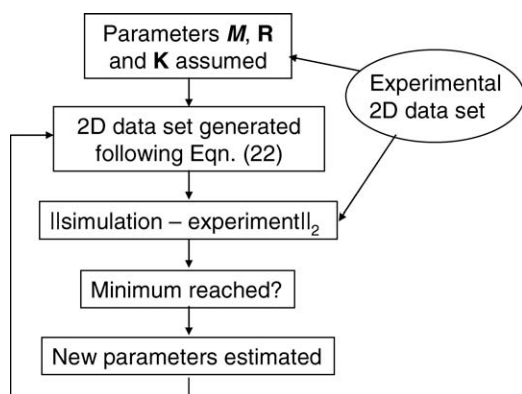


Figure 10 Flowchart demonstrating the procedure used to fit the experimental data. At each iteration, the simplex algorithm is used to estimate a new set of parameters minimizing the least-squares misfit of measured and experimental data points.

Table 4 Fit Parameters Obtained by the Simplex Algorithm

Parameter	Value
M^A	5.5
M^B	18.4
T_2^A	3.9 ms
T_2^B	103.5 ms
T_1^A	610 ms
T_1^B	630 ms
k	$1/110 \text{ ms}^{-1}$

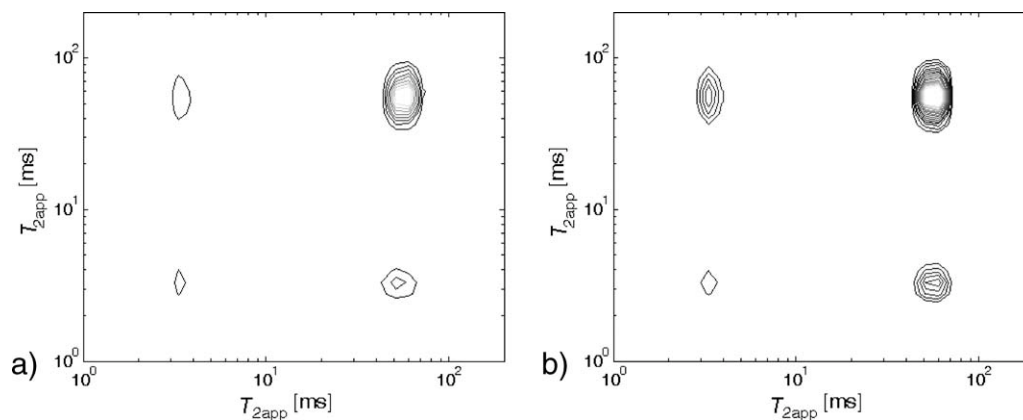


Figure 11 Experimental (a) and simulated (b) T_2 - T_2 exchange spectra of silica particles with the parameters of Table 3 for a mixing time of 70 ms.

this case, the single apparent T_1 corresponds to the nonzero eigenvalue of the $\mathbf{R}^{(1)} + \mathbf{K}$ matrix.

T_1 - T_2 correlation and T_2 - T_2 exchange experiments were performed with a homemade Halbach-magnet operating at a 21.85 MHz ^1H frequency. Using the algorithm described in section II, 2D time data set were simulated for two-site exchange with six different mixing times (0, 10, 30, 50, 70, and 90 ms). A simplex algorithm (28) was used to match the input parameters of the simulation with the experimental data for each mixing time. The data were first fitted directly in the time domain to avoid any artifact from the ILT. The fitting procedure is described in Fig. 10. The fit parameters are summarized in Table 4.

Although this is beyond the point of this study, it is interesting to note that the ratio of the observed amplitudes is 3.3. This is an order of magnitude below the expected value considering only the ratio between the interstitial space and the microporous volume. With a close packing volumetric density of 0.74 and porous volume within the particles of about 0.6% (a common

value for Stöber silica) (29), one should get a ratio of 43. There is thus a significant contribution of the surface water to the magnetization M_A .

Figure 11 shows the results obtained after ILT with a mixing time of 70 ms. One (a) is obtained by inverting the experimental data set, and the other one (b) by inverting the best-fit simulated data set. The peaks of the simulated maps are broader than the experimental ones. This is interpreted as a regularization artifact of the ILT procedure. To verify the quality of the fit, the evolution of the peak integrals with the mixing time for both simulated and experimental maps is compared in Fig. 12.

Except for a discrepancy concerning the diagonal peak 1 at low mixing time, Fig. 12 exhibits satisfactory agreement between the mixing time dependence of the peak intensities observed experimentally and the ones simulated using the parameters obtained by fitting the 2D data set. Thus, fitting experimental 2D time-domain data sets with simulated ones allows one to unravel relaxation from

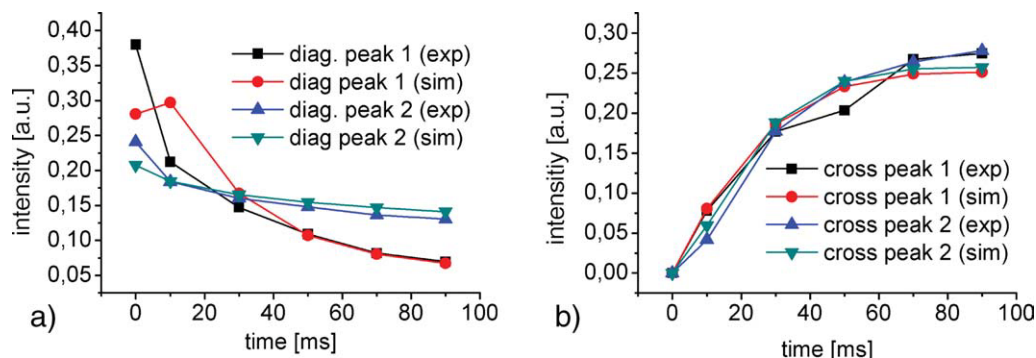


Figure 12 Comparison between the integrals of diagonal (a) and cross (b) peaks obtained by simulation and experiment versus the mixing time. [Color figure can be viewed in the online issue, which is available at www.interscience.wiley.com.]

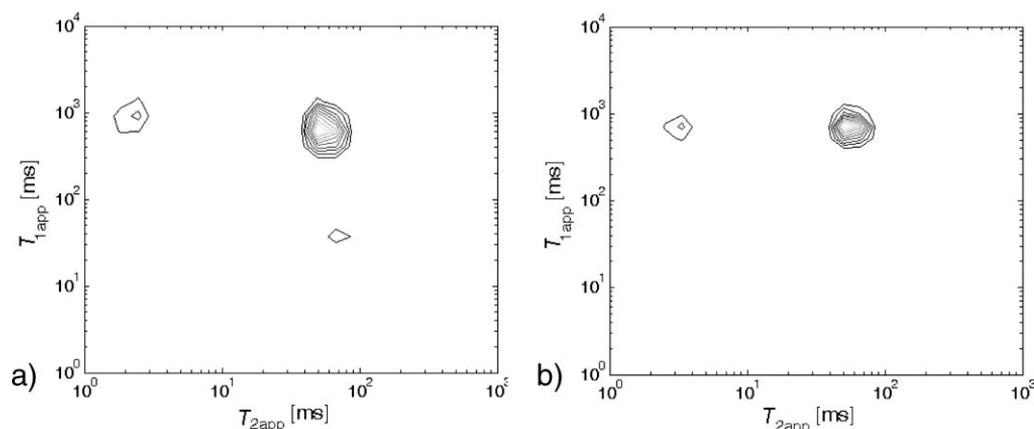


Figure 13 Experimental (a) and simulated (b) T_1 - T_2 correlation map of water-saturated silica particles derived with the parameters of Table 3.

exchange and obtain the true T_2 values, which are quite different from the apparent ones obtained by simple 1D fits [Fig. 9(a)]. Unfortunately, in the experimental system under study, it has not been possible to extract real T_1 values as the exchange time was too short to distinguish them.

In support of the exchange analysis, the T_1 - T_2 correlation map was measured and compared to the simulated one obtained with the fit parameters presented in Table 4 (Fig. 13). The small peak in the experimental map at low T_1 (around 40 ms) is likely to be noise and does not carry any meaning as the 1D fit of Fig. 9(a) clearly indicated a single T_1 .

V. CONCLUSION

In this work, we have shown that even if analytical solutions are known for two sites, a numerical simulation is required to analyze exchange maps with more than two sites. The simulations allowed us to propose a source for asymmetry, which is often observed experimentally as well as a source for the shift of peaks. Moreover, we proposed a method to extract the exchange kinetic parameters by fitting the experimental 2D time-domain data sets with simulated ones. As an example, two sites with an exchange rate of $1/110 \text{ ms}^{-1}$ were identified for water in a saturated dense packing of silica particles with a narrow particle size distribution.

Although the T_2 - T_2 exchange case has extensively been discussed, this approach can be easily extended to T_1 - T_2 correlation maps for which one example (Fig. 13) was given. Such experiments can be understood in terms of T_2 - T_2 experiments which start with T_1 encoding by saturation or inversion recovery instead of T_2 encoding in the evolution time, and where the mixing time vanishes.

The theoretical framework allows the study of n discrete-site systems, but its use is limited in practice to the case of four or five sites. Otherwise, the number of independent parameters becomes too large. On the other hand, it provides a first step toward the study of continuous distributions of sites.

ACKNOWLEDGMENTS

The authors express their gratitude to Prof. N. Lequeux (ESPCI) for the Stöber synthesis protocol as well as to Dr. Federico Casanova and Dr. Juan Perlo (RWTH) for truly helpful discussions. Financial support for this work was provided by Saint-Gobain Recherche (France) and TR32 (Germany).

REFERENCES

1. Hürlimann MD, Venkataraman L. 2002. Quantitative measurement of two-dimensional distribution functions of diffusion and relaxation in grossly inhomogeneous fields. *J Magn Reson* 157:31–42.
2. McDonald PJ, Mitchell J, Mulheron M, Aptaker PS, Korb JP, Monteilhet L. 2007. Two-dimensional correlation relaxometry studies of cement pastes performed using a new one-sided NMR magnet. *Cem Concr Res* 37:303–309.
3. Song YQ, Zielinski L, Ryu S. 2008. Two-dimensional NMR of diffusion systems. *Phys Rev Lett* 100:248002.
4. Washburn KE, Callaghan PT. 2006. Tracking pore to pore exchange using relaxation exchange spectroscopy. *Phys Rev Lett* 97:175502.
5. Callaghan PT, Arns CH, Galvosas P, Hunter MW, Qiao Y, Washburn KE. 2007. Recent Fourier and Laplace perspectives for multidimensional NMR in porous media. *Magn Reson Imaging* 25:441–444.

6. Callaghan PT, Godefroy S, Ryland BN. 2003. Diffusion-relaxation correlation in simple pore structures. *J Magn Reson* 162:320–327.
7. Chandrasekera TC, Mitchell J, Fordham EJ, Gladden LF, Johns ML. 2008. Rapid encoding of T-1 with spectral resolution in n-dimensional relaxation correlations. *J Magn Reson* 194:156–161.
8. McDonald PJ, Korb JP, Mitchell J, Monteilhet L. 2005. Surface relaxation and chemical exchange in hydrating cement pastes: a two-dimensional NMR relaxation study. *Phys Rev E* 72:011409.
9. Jeener J, Meier BH, Bachmann P, Ernst RR. 1979. Investigation of exchange processes by 2-dimensional NMR-spectroscopy. *J Chem Phys* 71:4546–4553.
10. Ernst RR, Bodenhausen G, Wokaun A. 1987. Principles of Nuclear Magnetic Resonance in One and Two Dimensions. Oxford: Oxford University Press.
11. Wüthrich K. 1995. NMR in Structural Biology. Singapore: World Scientific.
12. Macomber RS. 1998. A complete introduction to modern NMR spectroscopy. New York: Wiley.
13. McConnell HM. 1958. Reaction rates by nuclear magnetic resonance. *J Chem Phys* 28:430–431.
14. Bain AD. 2003. Chemical exchange in NMR. *Prog Nucl Magn Reson Spectrosc* 43:63–103.
15. Kroeker RM, Henkelman RM. 1986. Analysis of biological NMR relaxation data with continuous distributions of relaxation-times. *J Magn Reson* 69:218–235.
16. Lee JH, Labadie C, Springer CS, Harbison GS. 1993. Two-dimensional inverse Laplace transform NMR: altered relaxation times allow detection of exchange correlation. *J Am Chem Soc* 115:7761–7764.
17. Venkataramanan L, Song YQ, Hürlimann MD. 2002. Solving Fredholm integrals of the first kind with tensor product structure in 2 and 2.5 dimensions. *IEEE Trans Signal Process* 50:1017–1026.
18. Ernst RR, Anderson WA. 1966. Application of Fourier transform spectroscopy to magnetic resonance. *Rev Sci Instrum* 37:93–102.
19. Morris KF, Johnson CS. 1993. Resolution of discrete and continuous molecular-size distributions by means of diffusion-ordered 2D NMR-spectroscopy. *J Am Chem Soc* 115:4291–4299.
20. Callaghan PT, Manz B. 1994. Velocity exchange spectroscopy. *J Magn Reson Ser A* 106:260–265.
21. Sun BQ, Dunn KJ. 2005. A global inversion method for multi-dimensional NMR logging. *J Magn Reson* 172:152–160.
22. Hürlimann MD, Burcaw L, Song YQ. 2006. Quantitative characterization of food products by two-dimensional D-T-2 and T-1-T-2 distribution functions in a static gradient. *J Colloid Interface Sci* 297:303–311.
23. Monteilhet L, Korb JP, Mitchell J, McDonald PJ. 2006. Observation of exchange of micropore water in cement pastes by two-dimensional T-2-T-2 nuclear magnetic resonance relaxometry. *Phys Rev E* 74:061404.
24. Fleury M, Soualem J. 2009. Quantitative analysis of diffusional pore coupling from T2-store-T2 NMR experiments. *J Colloid Interface Sci* 336:250–259.
25. Whittall KP, Mackay AL. 1989. Quantitative interpretation of NMR relaxation data. *J Magn Reson* 84:134–152.
26. Straley C, Schwartz LM. 1995. Transverse Relaxation in Random Bead Packs: Comparison of Experimental Data and Numerical Simulations. Louvain, Belgium: Pergamon-Elsevier Science Ltd. pp 999–1002.
27. Green DL, Lin JS, Lam YF, Hu MZC, Schaefer DW, Harris MT. 2003. Size, volume fraction, and nucleation of Stober silica nanoparticles. *J Colloid Interface Sci* 266:346–358.
28. Nelder JA, Mead R. 1965. A simplex-method for function minimization. *Comput J* 7:308–313.
29. Szekeres M, Toth J, Dekany I. 2002. Specific surface area of Stoeber silica determined by various experimental methods. *Langmuir* 18:2678–2685.

BIOGRAPHIES



Maxime Van Landeghem was born in Paris (France) in 1984. He obtained his diploma from the French graduate school ParisTech National Institute of Physics and Chemistry (ESPCI ParisTech) in 2007 and his M.Sc. in 2008. Now, he is performing his PhD under the direction of Prof. Jean-Baptiste d'Espinose de Lacaillerie (ESPCI ParisTech) and Prof. Bernhard Blümich (RWTH). His PhD is focused on the understanding of drying and hydration process in porous media. He is funded by Saint-Gobain Research.



Agnes Haber was born in Covasna (Romania) in 1984. She obtained her B.Sc. (2006) and M.Sc. (2008) at Babes-Bolyai University in Cluj-Napoca (Romania). She is now doing her PhD at ITMC, RWTH Aachen, Germany, under the supervision of Prof. Dr. Bernhard Blümich. Her main research topic is focused on water dynamics in different porous materials by low-field NMR.



Jean-Baptiste d'Espinose de Lacaillerie is an assistant Professor at ParisTech National Institute of Physics and Chemistry (ESPCI ParisTech) in Paris. He is a member of the Soft Matter and Engineering Laboratory (a joint laboratory between ESPCI, the University Pierre et Marie Curie and the National Centre for Scientific Research). He holds a geological engineering diploma and a M.Sc. in Geochemistry from the National Institute of Geology (ENSPG INPL) in Nancy, France (1987) and a PhD. in Chemistry from the University of Wisconsin-Milwaukee (1992). He did his postdoctoral research at the French Petroleum Institute. He has coauthored more than 70 publications in the area of catalysis, surface chemistry of oxides in aqueous solutions, and solid-state NMR. His current research interests focus on the physics and chemistry of organomineral interactions at the nanoscale, the chemistry of cements substitutes for low carbon emission, and stray-field imaging of drying porous media.



Bernhard Blümich is Chair of Macromolecular Chemistry at RWTH Aachen University. His research interests are the development and applications of NMR for analysis of materials and processes. Starting with NMR as an undergraduate at the Technical University Berlin, he has since contributed to the methodological development of NMR in the areas of multidimensional stochastic NMR spectroscopy, solid-state NMR of polymers, NMR imaging of materials, and mobile NMR. He has published over 300 articles, edited six books, and written two monographs. In 2006, he was Miller Professor at the University of California at Berkeley, received the Ampere Price 2007 for the development of the NMR-MOUSE and its applications to various fields of science and technology, and was nominated Fellow of the International Society of Magnetic Resonance in 2008.